Received: 10 November 2021 | Revised: 22 June 2022 | Accepted: 25 June 2022

DOI: 10.1002/er.8361

RESEARCH ARTICLE

INTERNATIONAL JOURNAL OF ENERGY RESEARCH WILEY

A combined phenomenological artificial neural network approach for determination of pyrolysis and combustion kinetics of polyvinyl chloride

Gamzenur Özsin[1,2] | **Melis Alpaslan Takan**[3] | **Arda Takan**[4] | **Ayşe Eren Pütün**[5]

[1]Department of Chemical Engineering, Faculty of Engineering, Bilecik Şeyh Edebali University, Bilecik, Turkey

[2]Department of Chemical Engineering, Faculty of Engineering, Imperial College London, London, UK

[3]Department of Industrial Engineering, Faculty of Engineering, Bilecik Şeyh Edebali University, Bilecik, Turkey

[4]Department of Industrial Engineering, Faculty of Engineering, Eskişehir Technical University, Eskişehir, Turkey

[5]Department of Chemical Engineering, Faculty of Engineering, Anadolu University, Eskisehir, Turkey

Correspondence
Gamzenur Özsin, Department of Chemical Engineering, Faculty of Engineering, Bilecik Şeyh Edebali University, Bilecik, 11230, Turkey.
Email: gozsin@anadolu.edu.tr, gamzenur.ozsin@bilecik.edu.tr, g.ozsin@imperial.ac.uk

Funding information
Bilecik Şeyh Edebali University, Grant/Award Numbers: 2019-02.BŞEÜ.03-03, 2020-01.BŞEÜ.03-09

Summary

As a widely used plastic material polyvinyl chloride (PVC) accounts for a significant amount of plastic waste but also offers great potential in conversion to chemical feedstock via pyrolysis process. However, development of a sensitive mathematical approach is required for proper process design and monitoring of thermochemical conversion processes. In this work, we attempt to develop an artificial neural network (ANN) model for estimation of mass loss as a function of temperature and heating rate during pyrolysis and combustion of PVC. For this purpose, pyrolysis and combustion characteristics were quantified using thermogravimetric analysis, then non-isothermal kinetics were analysed by iso-conversional models. The results of ANN models show that this method helps predict complex systems with high regression coefficient (R^2) values. The best performed model analysed by ANN for pyrolysis was NN 7 with $R^2 = 0.9993$, the best performed model for combustion was NN 10 with $R^2 = 0.9982$. Comparison of experimental results to ANN predictions indicates that ANNs with a quick propagation algorithm can be an effective approach for modelling complex non-linear systems such as thermal degradation of thermoplastics.

KEYWORDS

artificial neural network (ANN), combustion, kinetics, polyvinyl chloride (PVC) polymer, pyrolysis

1 | INTRODUCTION

With ever-increasing population growth and modern lifestyle, plastics have evolved into one of the most widely-utilized materials in modern life due to polymer durability or reduced carbon dioxide emissions, related to lightness in weight. In parallel with the development of the polymer industry, the total world-wide production has exploded 183 times, increasing from 1.7 Mt in 1950 to 311 Mt in 2015. Furthermore, predictions estimate that another 33 billion tons of plastic materials will be produced and in circulation by 2050, if the current plastic manufacturing rates are maintained.[1] This considerable growth in the manufacturing and consumption of plastics and composite materials has resulted in a massive quantity of waste accumulation throughout the world and has created environmental concerns due to the non-biodegradable nature of plastics, and their adverse effects on the living organisms, ecosystems, plus safety.[2,3] With the use of appropriate and cost-effective recycling or

disposal procedures, plastic waste may become a significant source of energy and raw material feedstock. There are several technologies to overcome the problem of waste plastics, but each plastic disposal method has its own considerable pros and cons.[4] However, thermochemical conversion of waste to useful forms through waste-to-energy or waste-to-chemical routes, this offers several advantages that include simultaneous reduction of the secondary pollution problems and production of secondary fuel or chemicals.[5-7] As far as the other thermal treatments are concerned, pyrolysis, thermal degradation in an oxygen-deficient environment, presents further benefits of giving petroleum derivative chemicals or monomers and is a relatively easy and flexible process without intense sorting.[8-10] Pyrolysis is known to be an effective feedstock recycling method, where the organic waste is thermally cracked into hydrocarbon oils, carbonaceous char, and light hydrocarbon gases.[11-13] This thermochemical conversion method is especially beneficial for treating organic waste containing a mixture of long hydrocarbon chains whereby the long chains can be cracked into smaller chains.[14,15]

A global analysis of the results on plastics has shown that polyvinyl chloride (PVC) is utilized in the production of both short-life polymeric materials and composites, including cleansing materials, textiles, beverage bottles, healthcare devices, and long-lasting construction materials, such as floors coverings, piping, and windows due to its low cost and superior mechanical properties.[16,17] Moreover, as being a proton-donating polymer, applicability of PVC to form mixtures with other polymeric materials which act as plasticizers is advantageous.[18,19] Since PVC has such a wide range of products and industrial application fields, it has its significance in the entire plastics usage and end of life PVC wastes are accumulated worldwide. Meanwhile a huge potential exists in converting PVC wastes to chemical feedstock,[20-22] resins,[23] fuel grade intermediates,[24-26] and carbonaceous materials such as pitch, carbon fiber, and porous carbon[27-31] via pyrolysis process.

From both practical and economic points of view, it is required to simulate the degradation character of polymeric materials theoretically by mathematical approaches, before iterative testing with actual experimental systems. Upscaling thermochemical systems from laboratory to industry, necessitates a thorough understanding of kinetics to make accurate numerical predictions of thermal behaviors and optimize desired product yield.[32,33] TGA (thermogravimetric analysis) is a widely utilized technique that may be used to this end. Through exploration of effects and interactions between different process parameters, as well as parameter modeling and optimization, usage of TGA may allow a thorough understanding of the thermochemical conversion process which is an important step in upscaling and commercialization.[34] In recent years, artificial neural networks (ANNs) have also been applied to TGA data for interpretation of the thermal stability and mass loss-temperature relationships of materials during thermal degradation. For instance, ANNs have been applied to thermochemical conversion processes together with production of bio-based chemicals via biochemical processes.[35-37] The neural network might be used to determine and predict output results under various input situations through network training and testing. Therefore, ANNs serve as a useful and practical mathematical tool in thermal analysis and kinetic research.[38] It is not necessary to sketch the phenomena included between networks mathematically; learning and capability of the networks permit nonlinear and complex systems to update themselves during modeling.[39] The ANN method has been established in analogous with the brain's neural network and it has been applied in various thermally stimulated processes such as pyrolysis,[40,41] combustion,[42-44] and gasification.[45] In the field of polymer degradation and stability, inadequate research has been carried out using ANN. For instance, thermal degradation of cellulose, lignin, polyethylene, polyurethane, polyethylene[46-48] have investigated using ANNs. Yet, it is impossible to express a comprehensive model that links the kinetics of each polymer with its structure. Therefore, the wide range of polymeric materials should be investigated. Similar to other thermoplastics, PVC waste can be converted to value-added chemicals and energy by a sensible adjustment of thermal conversion processes for the economic and environmental sustainability. Although gaseous corrosive chlorine products during such kind of conversion are evolved, the emissions can be controlled by in-furnace methods such as catalysis, adsorption, and co-processing techniques.[49-52] Moreover, amidst the total of existing plastic wastes, PVC has a high amount in the volume sent to recycling and disposal.

Efforts to understand kinetic behavior of PVC in a faster, less complicated way using ANN may provide insights into the design, optimization, and upscaling of the thermal conversion processes. This study proposes ANN modeling to predict the kinetic information about the whole PVC pyrolysis and combustion process. The main focus and novelty of the study is to obtain trained models that may generate correct kinetic parameters without the need of conducting multiple experiments. Consequently, different functions were tested on TGA data obtained at variable heating rates and atmospheres. The best ANN architectures for pyrolysis and combustion processes were constructed using parameter tuning. Finally, kinetic parameters were calculated by different

models to conclude the capability of ANN in the estimation of kinetic parameters. The novelty of our study is in employing ANN for both pyrolysis and combustion of PVC and effectively using the final optimal design in the simulation of kinetic data such as activation energy.

2 | MATERIALS AND METHODS

2.1 | Sample collection, preparation and thermal analysis

PVC samples were gathered from a post-consumer waste plastic collection unit and the required particle size of 112 μm was obtained from screening the particles from the rotary mill using a screen. The particle size has been selected to ensure the internal temperature fluctuation of the particle can be ignored by assuming that there is a uniform temperature distribution inside the particle. For this purpose only particles with dimensionless Biot number that is less than unity were used. The Biot number compares convective heat transmission between a solid surface and its surroundings to heat transfer by conduction within a particle and with a very small Biot number a process is considered kinetically-limited for the purposes of the analysis. To minimize the thermal conduction effect within the sample, approximately 10 mg of PVC sample is taken in an Al_2O_3 crucible and evenly spread across the crucible. Nitrogen is purged initially to create an inert environment and then used to maintain an inert atmosphere during the pyrolysis runs. The experiment was conducted by heating samples from 25°C to 1000°C under a nitrogen flow rate of 20 cm^3/min using a TGA device (Setaram-Labsys Evo). The influence of heating rate was studied using linear heating rates ranging from 5 to 40°C/min. Selected heating rates were found proper to be used in the experiments, in order to visualize slow pyrolysis behavior and peak splitting. For combustion experiments, the same experimental conditions were maintained except changing gas flow to air during the heating period. Blank experiments were carried out to establish baselines and make corrections to minimize mass transfer effects. The resulting thermograms are percentages of remaining residue. Three runs for each experiment were performed to ensure accuracy and repeatability and an average curve was used for the kinetic calculations. Based on triplicates, the consistency of the TG data was approved with a deviation less than 0.12% and average results have been used in modeling. Before thermal analysis, PVC samples were characterized by ultimate analysis, proximate analysis, calorific value analysis and FT-IR spectroscopy. Procedures of ASTM, calorimeter bomb (IKA C200) and FT-IR spectrometer (Perkin Elmer Spectrum 100) together with chlorine determination based on Haslam and Soppet[53] were used for these purposes.

2.2 | Methodology of artificial neural network (ANN) modeling

The ANN model's uniqueness and advantage is its great accuracy. ANN learns from experimental data which has non-linear and multi-dimensional complex interactions by generalizing from an adequate amount of training data. Therefore, they are able to work as black-box models of multivariable static, and dynamic processes. Inspired by the functioning of the human brain, ANN structure is generally consisting of three parallel-connected layers of neurons as input, hidden, and output.[54-56] Each of these layers consists of a matrix of weight, a bias and output vector. The input and output layer numbers are equal to the parameter number and response number, respectively. The data gathering is generally performed outside of the network frame, and it has to be symbolical and all the data has to be changed in the limits in regard to variation margin for every variable. The transfer function of each layer and the conjunction between the layers and intermediate layer neurons are critical in terms of processing information. Frequently used transfer functions in ANN are linear (purelin), sigmoid or log-sigmoid, and hyperbolic tangent sigmoid[57] as it can be seen in supplementary file (S1).

Each of these layers consists of a matrix of weight, a bias and output vector. The input and output layer numbers are equal to the parameter number and response number, respectively. The data gathering is generally performed outside of the network frame, and it has to be symbolical and all the data has to be changed in the limits in regard to variation margin for every variable. The transfer function of each layer and the conjunction between the layers and intermediate layer neurons are critical in terms of processing information. Frequently used transfer functions in ANN are linear (purelin), sigmoid or log-sigmoid, and hyperbolic tangent sigmoid.[48] The studied data set in ANN is commonly classified in three sub-groups which are training, validation and testing set. The training process aims to adjust the neural synaptic weights to reach the steady-state. In order to obtain a correct model, the training data characteristics are crucial. The training data must be representative of the entire problem. In the proposed ANN model, input parameters that were utilized for the prediction of weight loss behaviors of PVC under inert and oxidative conditions for the determination of its pyrolysis and combustion behavior were heating rate and temperature. In this

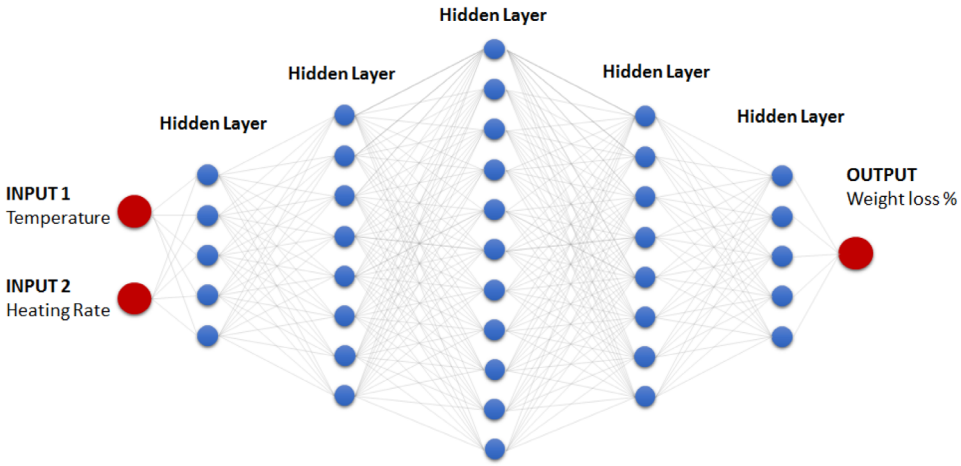

FIGURE 1 The structure of artificial neural network

study, more than 6500 lines of real experimental data were used, for the pyrolysis and combustion processes. As a standard 80% of the data is allocated for the training phase while 20% of the data is allocated for the validation process. Models with different complexity levels are discussed to determine accuracy. The used ANN architecture together with input and output parameters are mentioned in Figure 1.

2.3 | Kinetic analysis

A comprehensive understanding of thermal degradation reactions which include messy radical transformations together with complex product distribution is considered an obstacle. It is known that indefinite mechanisms and the lack of numerical rate constants for the reactions get in the way of their explicit description during mechanistic modeling. On the other hand, manual modeling of pyrolysis and combustion is exceptionally complex and time-consuming since they depend on several process factors and composition of the feedstock.[58,59] Extensive studies have concluded that the thermal degradation of polymeric materials is a complicated process and it may include various reactions in parallel and series. Hence, it is unreasonable to outline the overall process with a singular mechanism in most cases.[60] At this point, a widespread tool, thermogravimetric analysis (TGA), is beneficial to study the kinetics thermal degradation using either isothermal or dynamic conditions. Several analytical methods that utilize the TGA data are used to determine the kinetic parameters.[61-63] Amongst various approaches, isoconversional analysis may be performed at multiple heating rates in order to analyze the kinetics of the thermal degradation processes apart from the monitoring of the mass loss as a function of temperature during TGA runs.[64,65] In these methods, the activation energy is a function conversion which provides comprehensive knowledge during the entire thermal decomposition.[66] In this study, kinetic analysis has been performed along with the rules and suggestions of the Kinetics Committee of the International Confederation for Thermal Analysis and Calorimetry (ICTAC), which can be found in the literature.[67-69] In a simple manner, the principle of isoconversional approach was implemented for obtaining the variation of activation energy on conversion which remarks that the rate at constant conversion degree is only a function of the temperature solely, and that fractional conversion, $f(\alpha)$, is not dependent on the heating rate.

Kinetic studies in TGA is based on measuring sample mass as a function of temperature or time to calculate the dimensionless extent of reaction which is known as conversion degree, α, as follows:

$$\alpha = \frac{w_o - w_t}{w_o - w_f}. \quad (1)$$

In the equation, w_t represents the sample mass at time t, while w_o and w_f express sample masses at the initiation and termination of the reaction, respectively. In the case of linear heating rate of non-isothermal experimental modes, the sample mass was detected as a function of temperature. The basic rate equation specifies that the conversion is dependent on the temperature and concentration of reactants. The kinetics of the process using a linear heating rate (β) are described by temperature function ($k(T)$) and fractional conversion function ($f(\alpha)$) as shown in Equation (2):

$$\frac{d\alpha}{dt} = \beta \frac{d\alpha}{dT} = k(T) f(\alpha). \quad (2)$$

The rate constant, k, is depended on temperature according to the well-known Arrhenius equation as:

$$k(T) = A\exp\left(-\frac{E_a}{RT}\right). \quad (3)$$

In the Equation (3), E_a shows the activation energy and A represents the pre-exponential factor while R is the universal gas constant (R = 8.314 J/mol.K). After combining Equations (2) and (3), the reaction rate equation may be converted into:

$$\beta\frac{d\alpha}{dT} = A\exp\left(-\frac{E_a}{RT}\right)f(\alpha). \quad (4)$$

Equation (4) can also be converted into the Equation (5) after arrangements as:

$$\int_0^{\alpha}\frac{d\alpha}{f(\alpha)} = g(\alpha) = \frac{A}{\beta}\int_{To}^{T}\exp\left(-\frac{E_a}{RT}\right)dT \equiv \frac{AE_a}{\beta R}p(u). \quad (5)$$

$g(\alpha)$ and $p(u)$ are the integrated form of fractional conversion function $f(\alpha)$ and temperature integral, respectively. $p(u)$ is expressed as:

$$p(u) = \int_{\infty}^{u} -\frac{(\exp(-u))}{u^2}du, \quad (6)$$

where $u = E_a/RT$. Based on the kinetic methods applied, $p(u)$ can be expressed by some approximations, because $p(u)$ cannot be solved analytically. In the scope of this study Friedman[70] and Flynn-Wall-Ozawa (FWO),[71,72] KAS,[73,74] and Starink[75] models were employed to analyze kinetics of the pyrolysis and combustion processes. Equations (7)-(10) shows the linearized forms of the kinetic models using iso-conversional approach.

$$\ln\left(\beta\frac{d\alpha}{dT}\right) = \ln A + \ln f(\alpha) - \frac{E_a}{RT}\ (\text{for Friedman}), \quad (7)$$

$$\ln\beta = \ln\frac{AE_a}{Rg(\alpha)} - 5.331 - 1.052\frac{E_a}{RT}\ (\text{for FWO}), \quad (8)$$

$$\ln\left(\frac{\beta}{T^2}\right) = \ln\left(\frac{AR}{E_a g(\alpha)}\right) - \frac{E_a}{RT}\ (\text{for KAS}), \quad (9)$$

$$\ln\left(\frac{\beta}{T^{1.8}}\right) = C_s - 1.0037\frac{E_a}{RT}(\text{for Starink}). \quad (10)$$

It is known that advanced iso-conversional methods may determine the activation energies in respect to the whole conversion degree more precisely than general iso-conversional methods since they may reduce the influence of data noise.[76] One such method is devised by Vyazovkin, a kinetic approach that is quite precise and avoids the mistakes that come from approximating the temperature integral.[77] Vyazovkin's method overcomes the inaccuracies associated with the temperature integral's analytical approximation.[78]

TABLE 1 Characteristics of PVC waste

Ultimate analysis (wt.%)	C	47.91
	H	5.28
	N	0.38
	S	–
	[a]O	46.43
Proximate analysis (wt.%)	Moisture	0.28
	Ash	4.22
	Volatile	86.54
	[a]Fixed carbon	8.96
Heating value (MJ/kg)	21.16	
Chlorine content (wt.%)	[b]45.92	
FT-IR spectrum	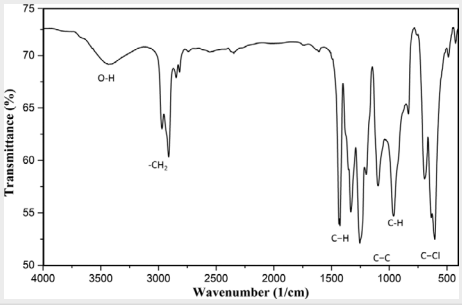	

[a]From difference.
[b]As-received basis.

$$\textbf{Vyazovkin}: \sum_{i=1}^{n}\sum_{j\neq i}^{n}\frac{I(E_\alpha, T_{\alpha,i})\beta_j}{I(E_\alpha, T_{\alpha,j})\beta_i} = \min, \quad (11)$$

where n is the number of heating rates and $I(E_\alpha, T_{\alpha,i})$ is the exponential integral. $I(E_\alpha, T_\alpha)$ function is given by:

$$I(E_\alpha, T_\alpha) = \int_0^{T_\alpha}\exp\left(\frac{-E_\alpha}{RT}\right)dT. \quad (12)$$

After estimation of activation energy, the pre-exponential factor values were then calculated by Kissinger's method using the calculated activation energy and peak temperature values as explained in Vyazovkin et al.[67] The calculations were performed via MS Excel and for the

Vyazovkin's method the relevant manuscript of Drozin et al.[79] has been assessed.

3 | RESULTS AND DISCUSSION

3.1 | Physicochemical characteristics of waste PVC

Table 1 shows the structure of as-received PVC waste according to several physicochemical characterization methods. Carbon was found to be the most prevalent element in the waste PVC structure, accounting for 47.91 wt. %, while chlorine accounted for 45.92 wt. %. Negligible nitrogen without any sulfur contents of the sample shows it will not produce NO_x and SO_x gasses during thermal degradation. According to the proximate analysis results, moisture, ash, and volatiles of the waste were 0.28, 4.22, and 86.54 wt%, respectively. According to the FT-IR spectrum of PVC, peaks at 2970 and 2911 cm^{-1} are consisting of the CH_2 asymmetric stretching vibration. The C − C stretching bond of the PVC backbone chain is observed in the range of 1000–1100 cm^{-1}. Peaks in the range of 600–650 cm^{-1} correspond to the C − Cl gauche bond while peaks near 850 cm^{-1} indicate C − Cl stretching. The peaks around 1400 cm^{-1} are assigned to the C − H aliphatic bending bond while trans CH wagging is observable at 962 cm^{-1}. The peak at 1255 cm^{-1} is attributed to the bending bond of C − H near Cl.[80,81] The O-H peak between 3100 and 3500 cm^{-1} demonstrates slightly absorbed water on the structure of the waste PVC.

3.2 | Thermal behavior of PVC in different heating rates and atmospheres

Mechanistically, it is widely known that PVC degradation is complex and it includes multiple degradation pathways. The two stages of the PVC pyrolysis are shown in Figure 2 and it contains two main mass loss zones plus a long shoulder at below and above approximately 515°C. The mass loss zones are corresponding to dTG peaks and their onset and offset values in sequence according to the Figure 2. The temperature range of main pyrolysis reactions of PVC was recorded between 235°C and 578°C. PVC pyrolysis is started with HCl elimination or dehydrochlorination at lower temperatures which is initiated by the scission of the Cl − C bond, resulting in a chlorine radical. The dehydrochlorination step causes the formation of conjugated double bonds and polyene radicals with some hydrocarbon formation, particularly evolution of unsubstituted aromatic hydrocarbons may be observed in this stage. HCl, a little quantity of benzene, alkyl aromatic hydrocarbons (toluene, xylene isomers, ethylbenzene, etc.), and condensed ring aromatic hydrocarbons are the results at this step (naphthalene, indene, indene, etc.).[82,83] The evolution of HCl is significant in the

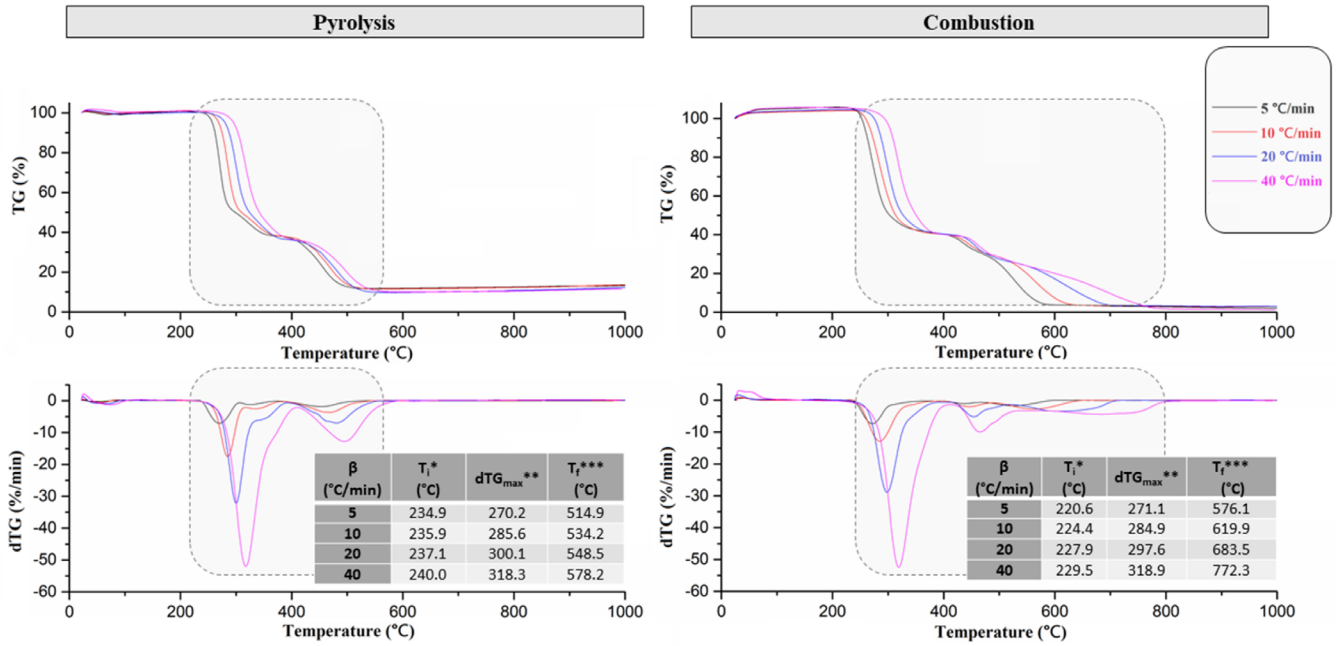

FIGURE 2 TG and dTG curves for Polyvinyl chloride pyrolysis and combustion with characteristic temperatures (T_i: initial temperature of the main thermal degradation zone, dTG_{max}: peak temperature of dTG curve, and T_f:final temperature of the main thermal degradation zone)

pyrolysis of PVC since degradation follows an autocatalytic dehydrochlorination pathway with the succeeding conjugated pi bond formation.[84,85] In other words, HCl formed during dehydrochlorination can further catalysis the decomposition and thus generate polyene sequence. It is known that the release of HCl gas makes allylic chlorine more active in the polymer backbone and unzipping initiates until the conjugation is stabilized by resonance itself. By increasing temperature, the conjugated structures increase the formation of volatile aromatic compounds and the decomposition goes along with cracking into low hydrocarbons with linear or cyclic structure.[85,86] Therefore, the formation of alkyl aromatics with some char formation occurs because of condensation and dehydrogenation with severe dealkylation, isomerization, chain scission, crosslinking, and aromatization after the dehydochlorination step. Eventually, aromatic and polyaromatic compounds and a small amount of char are generated after the main thermal degradation zone PVC in an inert atmosphere.[87] As a consequence of these reactions, PVC underwent two main degradation zones during pyrolysis with some overlapping peaks. Some adjacent mass loss peaks in dTG curves overlapped when the heating rate was raised. When the heating rate increased to 40°C/min, the two peaks merged into one at a temperature between 235°C and 410°C. At the end of pyrolysis PVC decomposed almost completely with a minor amount of residue due to the presence of additives. Approximately 11 wt.% of solid residue remained at 1000°C after thermal degradation in the nitrogen atmosphere.

The thermograms of PVC combustion bears a striking dissimilarity to the pyrolysis thermograms, indicating that different mechanisms of decomposition occur under the air atmosphere. In combustion experiments, PVC exhibited three peaks which were related to a three-stage degradation process. Dehydrochlorination, degradation of the carbonaceous chain, and secondary carbonization stages were observed by successive three thermal degradation zones. For PVC combustion, a three-staged thermal decomposition was noticed showing the char formation and char combustion in the final stage at higher temperatures. It was detected that the last stage, which is known as char combustion or secondary carbonization, occurred in the range of 495°C–772°C depending on the applied heating rate with a mass loss of more than 25 wt. %. Moreover, combustion of the PVC was initiated at lower temperatures than pyrolysis for all heating rates. This may be explained due to the effect of oxygen in accelerating the rapid volatilization.[88] It is noteworthy that oxidative thermal decomposition of PVC during combustion also facilitated the devolatilization, resulting in a lower weight fraction of residual char. Solid residue remained after PVC combustion is much less than the residue of pyrolysis experiments which is approximately 2 wt. %. Catalytic effect of oxygen, especially during the hydrogen chloride elimination stage may be responsible for this remarkable weight loss, as is concluded by Valko et al.,[89] and the occurrence of the last char combustion stage. All in all, some oxidation reactions are anticipated to form volatile products such as CO_2, CO, H_2O, and oxygen-containing compounds in an air atmosphere. Hence, and hence thus much less residue achieved after combustion than pyrolysis.

Several studies have investigated char formation mechanism during the thermal degradation of PVC. For instance, XRD examination of solid residues at 400°C by Ye et al.[90] revealed that there are not any peaks that could be attributed to PVC while char showed that thermal degradation resulted in the formation of net-like carbon structures. On the other hand, XRD characterization of char at 800°C indicated carbon as the ultimate solid product of complete degradation. Radical species produced by the intramolecular HCl production mechanism might react with adjacent PVC backbones to generate a cross-linked carbonaceous structure. As a result, it can be inferred that cross-linking by the intramolecular HCl formation contributes to char formation. Masuda et al.[91] also concluded partial development of layered graphite structure by the characterization of PVC after degradation. Aso et al. also investigated structural characteristics of the solid residues remained after thermal degradation of PVC with respect to temperature and characterized the char obtained at different temperatures from 500 to 1000°C in detail. With the help of detailed characterization techniques including elemental analysis, x-ray diffraction (XRD), high resolution transmission electron microscopy (HRTEM) and temperature programmed oxidation (TPO); reactivity and structure of the chars at different temperatures were analyzed. They confirmed evolution of H_2O, CO_2 and CO during thermal degradation and enhancement of the carbon content during decomposition. Moreover, XRD and TEM investigations showed that formation of planar aromatic sheets and number of stacking tends to increase while inter-atomic spacing (d-spacing) remains constant during thermal degradation from 500°C to 1000°C.[92] Other than carbonaceous structure, the presence of metal compounds in the residue of waste PVC after thermal decomposition might be oxides or inorganic additives such as calcium carbonate and might contribute crystal phase composition of the char.[93,94]

According to the TGA results, the combustion residue is found to be slightly higher than the pyrolytic char residue at 350°C which is similar to the study of Bittencourt et al. As they have explained, this may be as a result of

TABLE 2 ANN models tested for the pyrolysis and combustion processes and regression performance results

Models	Network structure	Heating rates for training	Heating rate for test	Transfer function	Test R^2 Score		Validation R^2 Score	
					Pyrolysis data set	Combustion data set	Pyrolysis data set	Combustion data set
NN 1	5-10-5	5°C/min 10°C/min 20°C/min	40°C/min	Tansig	0.9397	0.7560	0.9621	0.7578
NN 2	5–10-5	5°C/min 10°C/min 40°C/min	20°C/min	Sigmoid	0.9156	0.7450	0.9582	0.7457
NN 3	5-30-5	5°C/min 20°C/min 40°C/min	10°C/min	Tansig	0.9697	0.7760	0.9714	0.7777
NN 4	10–20-10	10°C/min 20°C/min 40°C/min	5°C/min	Sigmoid	**0.9990**	0.7451	0.9999	0.7460
NN 5	10–20-10	5°C/min 10°C/min 40°C/min	20°C/min	Sigmoid	**0.9977**	0.7333	0.9992	0.7342
NN 6	10–20-10	10°C/min 20°C/min 40°C/min	5°C/min	Tansig	**0.9991**	0.8325	0.9999	0.8345
NN 7	10–20-10	5°C/min 20°C/min 40°C/min	10°C/min	Tansig	**0.9993**	0.8524	0.9999	0.8550
NN 8	5–10–20-10-5	5°C/min 10°C/min 20°C/min	40°C/min	Sigmoid	0.7755	0.9124	0.7775	0.9152
NN 9	5–15-30-15-5	5°C/min 20°C/min 40°C/min	10°C/min	Tansig	0.7756	0.9723	0.7770	0.9741
NN 10	5–20-30-20-5	5°C/min 20°C/min 40°C/min	10°C/min	Tansig	0.6533	**0.9982**	0.6540	0.9998
NN 11	1–3-1	5°C/min 10°C/min 20°C/min	40°C/min	Sigmoid	0.7887	0.6242	0.7422	0.6126
NN 11	1–3-1	5°C/min 10°C/min 20°C/min	40°C/min	Sigmoid	0.7887	0.6242	0.7422	0.6126

Note: Significant results are presented in bold.

the production of thermally stable non-volatile compounds in an oxidizing environment.[95] Another important observation on the differences between PVC combustion and pyrolysis is that combustion exhibited a wide mass loss temperature range when it is compared with pyrolysis. It is most likely that in the combustion of PVC, the heating rate is the decisive factor to the termination temperature since differences in termination temperature in combustion are higher than that of pyrolysis. It may indicate that char oxidation requires further time at the last stage of combustion.

For both pyrolysis and combustion of PVC, the initial degradation temperature was repositioned to the higher temperatures and the peaks became sharper by increasing the heating rate. As the heating rate increases, the peak temperature increases accordingly as can be seen from thermograms. The increment of heating rate hindered the pyrolysis and combustion products on the surface to diffuse, thereby postponing the internal thermal degradation and resulting in thermal hysteresis (or thermal lag). Thermal hysteresis is a known phenomenon as a result of heat transfer limitation; occurring as a

TABLE 3 Comparison of the statistical parameters as Mean squared error (MSE), root MSE (RMSE) and mean absolute error (MAE) of different artificial neural network (ANN) models

Model Structure	Number of Layers	Total Number of Neurons	Complexity level	MSE-Pyrolysis	MSI-Combustion	RMSE-Pyrolysis	RMSE-Combustion	MAE-Pyrolysis	MAE-Combustion
1-3-1	3	5	1	0.0012	0.0019	0.0351	0.0436	0.0315	0.0409
2-5-2	3	9	2	0.0008	0.0020	0.0282	0.0446	0.0293	0.0459
5-5-5	3	15	3	0.0005	0.0016	0.0233	0.0397	0.0233	0.0381
5-10-5	3	20	4	0.0005	0.0017	0.0217	0.0410	0.0225	0.0414
5-20-5	3	30	5	0.0003	0.0010	0.0180	0.0315	0.0173	0.0325
5-30-5	3	40	6	0.0004	0.0008	0.0208	0.0288	0.0194	0.0300
10-20-10	3	40	7	0.0003	0.0012	0.0159	0.0345	0.0145	0.0325
5-10-20-5	4	40	8	0.0005	0.0006	0.0233	0.0244	0.0242	0.0234
5-15-15-5	4	40	9	0.0008	0.0005	0.0282	0.0233	0.0265	0.0226
5-20-10-5	4	40	10	0.0008	0.0006	0.0275	0.0248	0.0273	0.0235
5-10-20-10-5	5	50	11	0.0012	0.0002	0.0345	0.0128	0.0314	0.0133
5-15-30-15-5	5	70	12	0.0009	0.0002	0.0307	0.0147	0.0282	0.0138
5-20-30-20-5	5	80	13	0.0012	0.0001	0.0345	0.0104	0.0321	0.0101
10-20-20-20-10	5	80	14	0.0024	0.0005	0.0488	0.0233	0.0503	0.0221
10-20-30-20-10	5	90	15	0.0028	0.0003	0.0528	0.0180	0.0491	0.0189
10-30-35-30-10	5	115	16	0.0036	0.0004	0.0598	0.0208	0.0592	0.0200
15-20-20-20-20-15	6	120	17	0.0036	0.0009	0.0601	0.0301	0.0547	0.0304
15-20-25-25-20-15	6	130	18	0.0031	0.0020	0.0561	0.0446	0.0510	0.0432

Notes: $\mathrm{MSE} = \frac{1}{N}\sum_{m=1}^{N} {e_m}^2$.

$\mathrm{RMSE} = \sqrt{\frac{1}{N}\sum_{m=1}^{N} {e_m}^2}$.

$\mathrm{MAE} = \frac{1}{N}\sum_{m=1}^{N} |e_m|$.

N: size of the data set.

e_m: error value.

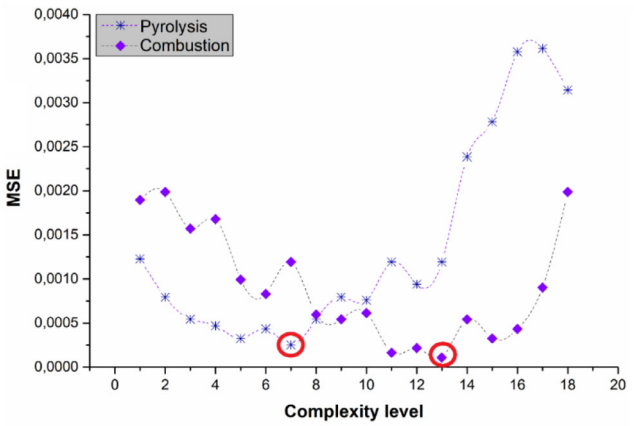

FIGURE 3 Best performing artificial neural network models of pyrolysis and combustion by complexity level

result of temperature difference along the sample section. The sample is known to require higher temperatures to degrade at higher heating rates. In the use of higher heating rates, the reactions take a certain time for pyrolysis and combustion, shortening the reaction time for samples that are not conducive to the heat transfer.[96,97] The maximum peak temperatures for pyrolysis were 270.2°C, 2856°C, 300.1°C, and 318.3°C for heating rates of 5°C, 10°C, 20°C, and 40°C/min, respectively. Meanwhile, the maximum peak temperatures of combustion at 5°C, 10°C, 20°C, and 40°C/min was 271.1°C, 284.9°C, 297.6°C, and 318.9°C, respectively exhibiting an increasing trend with the heating rate like pyrolysis process. By increasing the heating rate from 5 to 40°C/min, the rate of maximum thermal degradation is raised from 7.02 to 52.04%/min for pyrolysis while it is changed from 7.33 to 52.46%/min for combustion.

3.3 | ANN model development and performance

In the scope of studies regarding the thermal degradation process with the ANN approach, the analyzed data can be separated randomly into 3 subgroups for training, validation, and test processes.[98] However, the aim is to minimize the number of experiments by using ANN model in this study. To this end, several combinations of heating rates among a total of four different heating rates were used for the prediction of the others during training. The studied ANN model was created with Python programming language utilizing Keras library which uses Tensorflow backend. For the backpropagation process, an Adam optimizer was used. Two different transfer functions which are tansig and sigmoid were applied and 20% of the random data sets were split for the training and the validation processes indiscriminately. In order to demonstrate the applicability of ANN models to real-life scenarios, the data set was split into two parts for the training and test phases. The two parts consist of data that have different heating rates, so that the estimation of a heating rate that was not used during the training phase, would indicate the realistic features of ANN models. This procedure reduces the risk of overfitting for the studied data. The network models were subjected to 1000 iterations with a target error of 10^{-6} and multiple runs were generated for different parameters to compare the neural models. Different structures with varying numbers of layers and neurons were tested during multiple runs, the parameters used and the obtained results for two different data of pyrolysis and combustion experiment sets are presented in Table 2. The table summarizes the unique number of neural structures, details of the regarding neural structure together with the combination of heating rate data used during training, validating and testing processes. Moreover, transfer functions used in the model, test, and validation regression coefficient (R^2) scores of pyrolysis and combustion were given in the table. For the evaluation of the performance R^2 score was calculated. In general, the R^2 values are evaluated in three ranges. $R^2 > 0.9$ shows desirable performance and R^2 values between 0.8 and 0.9 indicates fair performance while $R^2 < 0.8$ implies unsatisfying performance for modeling.[99] According to the outputs, the best-performed neural network model for pyrolysis data was NN 7 with tansig transfer function with 3 layers (10-20-10) with a R^2 value of 0.9993. When it comes to the combustion process, the best neural network model was NN 10 with tansig transfer function with 5 layers (5-20-30-20-5) with R^2 value of 0.9982. Since mechanisms lying behind the thermal degradation of pyrolysis and combustion are different, it results in some kind of mathematical complexities in model development and hence, the same neural structure gives different performance results for different data sets. Pyrolysis data set performed better results with simpler neural structure while combustion data set gave better results with a relatively more complex neural structure. For instance, the NN 4 model with 3 layers and 10, 20, 10 neuron numbers, gave better results for the test of pyrolysis data with R^2 score of 0.9990 while the model performed poorly for combustion data with R^2 score of 0.7451. In a similar manner, a relatively more complex NN 10 model (with 5 layers and a larger number of neurons), performed better results for the combustion data with R^2 score of 0.9982 while the R^2 score was 0.6533 for the pyrolysis data.

In order to elaborate the performance results of different ANN models, tests were performed with the same parameters such as transfer function and heating rate to

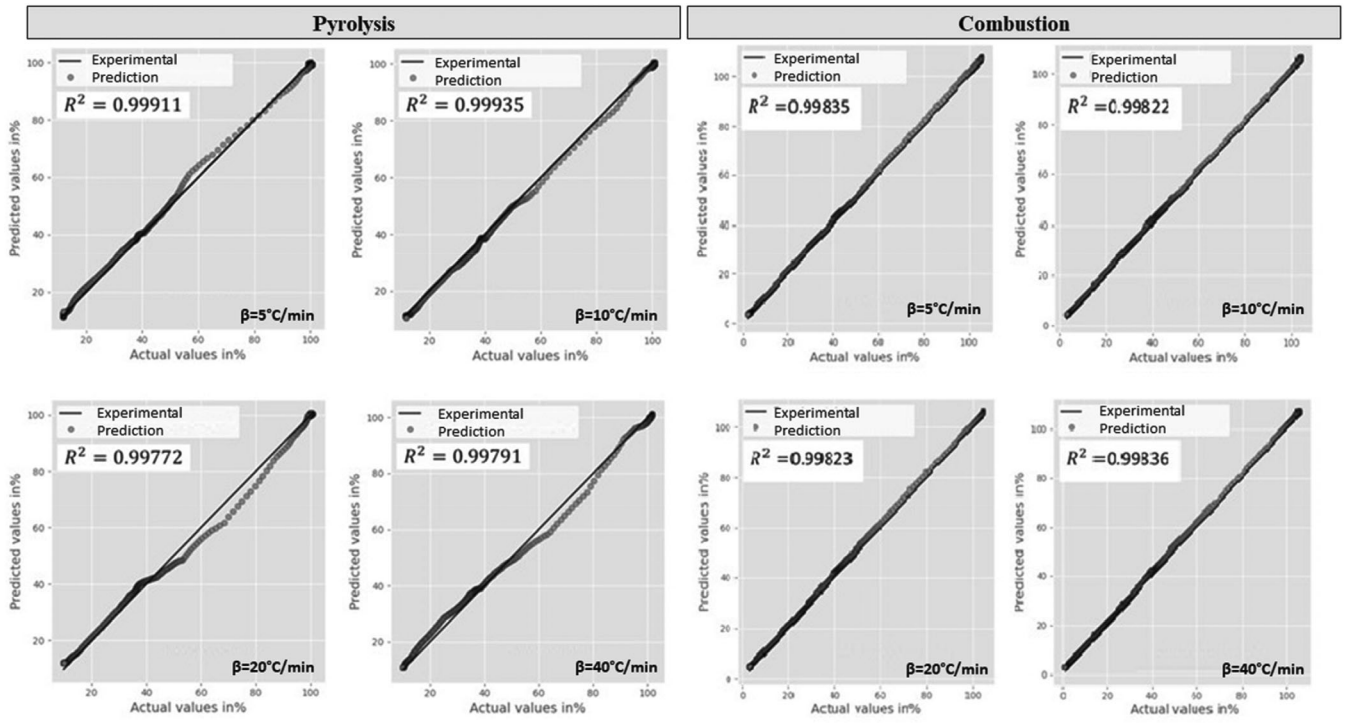

FIGURE 4 The comparison of the experimental data and predicted data for pyrolysis and combustion data sets

be estimated. For all test runs, tansig function was used and 5, 10, and 20 heating rates were used in the training process and TG data for 40 heating rates were predicted. Model structures were created with different numbers of hidden layers and neuron numbers. Since the regression model of the TGA is a complex polynomial function with relatively low number of parameters (in this case: 2 inputs-1 output) it requires higher complexity from the ANN model. Mean squared error (MSE), root mean square error (RMSE), and mean absolute error (MAE) were employed as performance indicators. TG data was normalized to 0–1 range to emphasize the results of the performance indicators. From these models, only stable models with relatively higher performance were selected. Details of the statistical results are represented in Table 3. In order to compare different structures, a complexity level was introduced. The complexity level is increased with both the number of hidden layers and the number of neurons in total. For example, the model 5-10-5 with complexity level 4 has 3 hidden layers and 20 neurons in total while 5-20-5 with complexity level 5 has also 3 hidden layers but 40 neurons in total. The MSE values in Table 3 for the pyrolysis varied from 0.0003 to 0.0036 while for the combustion, it changed from 0.0001 to 0.0020. The RMSE values are between 0.0159 and 0.0601 for pyrolysis, 0.0104 and 0.0446 for combustion. MAE also changed from 0.0145 to 0.0592 for pyrolysis and it varied from 0.0101 to 0.0459 for combustion. The minimum MSE, RMSE and MAE values for pyrolysis were calculated for the model structure 10-20-10 with the complexity level 7 and 40 neurons. The minimum MSE, RMSE and MAE values for combustion were calculated for the model structure 5-20-30-20-5 with the complexity level 13 and 80 neurons. The performances of the models are similar to the models presented in Table 2 as expected. Figure 3 shows the best performing ANN models among the randomly selected models for both pyrolysis and combustion processes.

Figure 4 demonstrates the comparison of the experimental data and predicted data for different heating rates of PVC pyrolysis and combustion data set, respectively. Furthermore, the experimentally-observed and predicted TG curves are compared in the supplemental files (S2 and S3) for PVC pyrolysis and combustion at different heating rates. It is remarkable that the results obtained from the analysis demonstrated the power of ANNs for the prediction of the results in thermal degradation experiments. It is inevitable to say that further weight loss data with different parameters can be realistically predicted with the obtained experimental results by the help of ANN.

3.4 | Kinetic analyses based on different iso-conversional methods

The practical use of polymers such as PVC requires accurate knowledge of operating temperature and thermal

TABLE 4 Comparison of activation energy calculated by Friedman, Flynn-Wall-Ozawa (FWO), KAS, and Starink iso-conversional methods

	Pyrolysis				Combustion			
	Experimental		Prediction		Experimental		Prediction	
α	E_a (kj/mol^{-1})	R^2	E_a (kj/mol^{-1})	R^2	E_a (kj/mol^{-1})	R^2	E_a (kj/mol^{-1})	R^2
Friedman								
0.1	94.8	0.9961	110.7	0.9893	114.4	0.9961	106.4	0.9859
0.2	95.7	0.9995	105.3	0.9953	115.8	0.9875	114.8	0.9848
0.3	92.1	0.9999	111.5	0.9999	116.0	0.9988	118.0	0.9944
0.4	116.9	0.9986	116.1	0.9826	113.6	0.9735	112.7	0.9776
0.5	106.5	0.9942	110.0	0.9835	127.3	0.9966	111.6	0.9812
0.6	183.0	0.9992	185.8	0.9913	193.7	0.9981	187.5	0.9998
0.7	234.1	0.9920	233.4	0.9911	132.8	0.9916	149.5	0.9985
0.8	227.9	0.9769	225.8	0.9968	105.1	0.9854	101.9	0.9628
0.9	212.8	0.9986	213.2	0.9885	68.5	0.9859	59.8	0.9566
$\bar{x}$	**151.5**	0.9950	**156.9**	0.9910	**120.8**	0.9900	**118.0**	0.9820
FWO								
0.1	128.4	0.9997	118.5	0.9840	125.6	0.9945	119.3	0.9933
0.2	117.7	0.9990	120.0	0.9962	111.1	0.9887	111.9	0.9884
0.3	113.0	0.9997	117.0	0.9992	111.5	0.9978	113.7	0.9972
0.4	109.6	0.9998	118.1	0.9971	115.9	0.9881	115.8	0.9887
0.5	108.2	0.9997	118.2	0.9807	144.3	0.9836	143.9	0.9903
0.6	147.0	0.9957	160.2	0.9982	137.6	0.9983	123.1	0.9961
0.7	260.9	0.9971	176.9	0.9965	109.9	0.9979	126.1	0.9859
0.8	240.1	0.9991	241.6	0.9868	115.3	0.9995	144.4	0.9913
0.9	224.4	0.9991	222.1	0.9958	140.3	0.9939	123.2	0.9936
$\bar{x}$	**161.0**	0.9990	**154.7**	0.9930	**123.5**	0.9940	**124.6**	0.9920
KAS								
0.1	125.9	0.9997	115.4	0.9814	123.1	0.9936	116.3	0.9921
0.2	114.4	0.9988	116.9	0.9955	107.5	0.9864	108.3	0.9861
0.3	109.4	0.9996	113.6	0.9990	107.8	0.9973	110.2	0.9966
0.4	105.8	0.9998	114.8	0.9965	112.3	0.9857	112.2	0.9865
0.5	104.1	0.9996	114.7	0.9777	141.5	0.9809	141.0	0.9887
0.6	144.6	0.9950	158.5	0.9980	135.1	0.9981	119.7	0.9954
0.7	263.7	0.9969	175.1	0.9961	103.4	0.9974	128.1	0.9831
0.8	240.5	0.9991	242.0	0.9855	108.1	0.9993	138.6	0.9898
0.9	223.5	0.9990	221.0	0.9953	133.1	0.9927	115.1	0.9922
$\bar{x}$	**159.1**	0.9990	**152.5**	0.9920	**119.1**	0.9920	**121.1**	0.9900
Starink								
0.1	126.3	0.9997	115.9	0.9817	123.5	0.9937	116.8	0.9922
0.2	114.9	0.9988	117.4	0.9955	108.0	0.9867	108.9	0.9864
0.3	110.0	0.9996	114.2	0.9991	108.3	0.9974	110.7	0.9966
0.4	106.3	0.9998	115.3	0.9966	112.8	0.9860	112.7	0.9868
0.5	104.7	0.9997	115.2	0.9780	142.0	0.9812	141.5	0.9888
0.6	145.0	0.9951	158.9	0.9980	135.5	0.9981	120.3	0.9954

TABLE 4 (Continued)

	Pyrolysis				Combustion			
	Experimental		Prediction		Experimental		Prediction	
α	E_a (kj/mol^{-1})	R^2	E_a (kj/mol^{-1})	R^2	E_a (kj/mol^{-1})	R^2	E_a (kj/mol^{-1})	R^2
0.7	263.8	0.9969	175.6	0.9961	104.2	0.9974	121.3	0.9834
0.8	240.8	0.9991	242.3	0.9856	109.0	0.9993	139.4	0.9900
0.9	224.0	0.9999	221.4	0.9953	134.0	0.9929	116.1	0.9924
$\bar{x}$	**159.5**	0.9990	**152.9**	0.9920	**119.7**	0.9930	**120.9**	0.9900

Note: Significant results are presented in bold. $\bar{x}$: Mean value.

TABLE 5 Values of activation energy calculated by advanced Vyazovin method

	Pyrolysis		Combustion	
	Experimental	Prediction	Experimental	Prediction
α	E_a(kj/mol^{-1})	E_a(kj/mol^{-1})	E_a(kj/mol^{-1})	E_a(kj/mol^{-1})
0.1	98.8	100.0	112.9	109.4
0.2	95.2	97.8	107.0	108.0
0.3	111.1	111.0	107.1	110.0
0.4	114.0	114.0	112.0	112.0
0.5	110.0	112.0	134.9	137.9
0.6	156.8	157.9	131.7	129.7
0.7	253.9	174.7	112.9	109.8
0.8	229.9	227.9	107.0	116.8
0.9	211.9	213.0	107.0	107.7
$\bar{x}$	153.5	145.4	114.7	115.7

Note: $\bar{x}$ Mean value.

lifespan matching to a certain end-point criterion. By considering thermal behavior during combustion and pyrolysis it is possible to interpret the degradation mechanism and the stability. ANN model used in the current study is implemented to different heating rates that is, 5, 10, 20 and 40°C/min to model the pyrolytic and oxidative decomposition behavior of PVC successfully. By virtue of the multiple degradation stages, pyrolysis and combustion of the PVC underwent complex reactions. According to the results, a significant distinction between the pyrolysis and combustion processes of PVC existed. This shows that the presence of oxygen that led to oxidative degradation could significantly influence the kinetics of the process. To further understand the applicability of ANN on kinetics, experimentally determined activation energy values which were calculated by the help of TGA data were compared with the model predictions as shown in S2 and S3. The experimental data was fitted by the isoconversional Friedman, Flynn-Wall-Ozawa, Kissinger-Akahira-Sunose, and Starink models to acquire the kinetic parameters, whilst the predicted kinetic constants were obtained by replacement of the weight loss and corresponding conversion degree found from the ANN models into the analytical model. The minimum energy quantity required to start a chemical reaction or to produce an activated complex, which is regarded as an intermediate step between reactants and products, is known as activation energy. The lower values of activation energies indicate higher reaction rates that can be achieved by providing lower energy. For instance, the lower the activation energy value for combustion is related with higher flammability. The corresponding activation energy values with regression coefficient (R^2) are reported in Table 4. The model predictions are in good agreement with the experimentally determined profiles. Results have shown that the trends of predictions of ANN as a function of conversion degree agrees with the experimentally found activation energy values using different isoconversional methods. In terms of the kinetic models and ANN, the mean value of activation energy did not differ

significantly. The maximum difference in the experimental and predicted mean value of activation energy was about 6.6 kj/mol. Moreover, the relationship between the activation energy and the conversion revealed similar tendencies, which proved the accuracy of the calculation methods.

When considering average activation energy determined for pyrolysis and combustion, pyrolysis seems to require higher energy than combustion which confirmed that presence of oxygen influences kinetics as well as the mechanism. Notably, in the initial stage of degradation ($0 < \alpha < 0.2$) lower activation energy values of pyrolysis compared with combustion indicates that initiation of dichlorination is easier in an inert atmosphere. The lowest activation energy requirements to start combustion were found to be 94.8 kJ/mol. by the Friedman method. On the other hand, lower activation energy values in combustion are noticeable at higher conversion degrees after a point of 0.7. The degradation of PVC in air might therefore be enhanced by molecular oxygen through radical interactions at the last termination stage.

In chemical kinetics, the almost constant activation energy values throughout the conversion degree indicate a uniform energetic demand, while variations in activation energy are thought to be caused by the complexity of reaction schemes. The results showed an observation relating to severe fluctuations of the activation energy on the conversion which implies complex degradation mechanisms during both pyrolysis and combustion. Considering the respective dependency of activation energy to the conversion degree, combustion showed a different degradation mechanism than pyrolysis due to oxidative reactions occurring in the air, as expected.

For pyrolysis, the activation energy values varied between 92.1 and 234.1 kJ/ mol with an average of 151.5 kJ/ mol based on the Friedman method while the predicted average pyrolysis activation energy was 156.9 kJ/ mol. In the study of Liu et al.[100] the activation energy values were calculated using the FWO technique at various conversion degrees and the values were ranged from 132.8 and 266.4 kJ/mol while Xu et al.[101] found activation energy between 48.1 and 113.6 kJ/mol using the

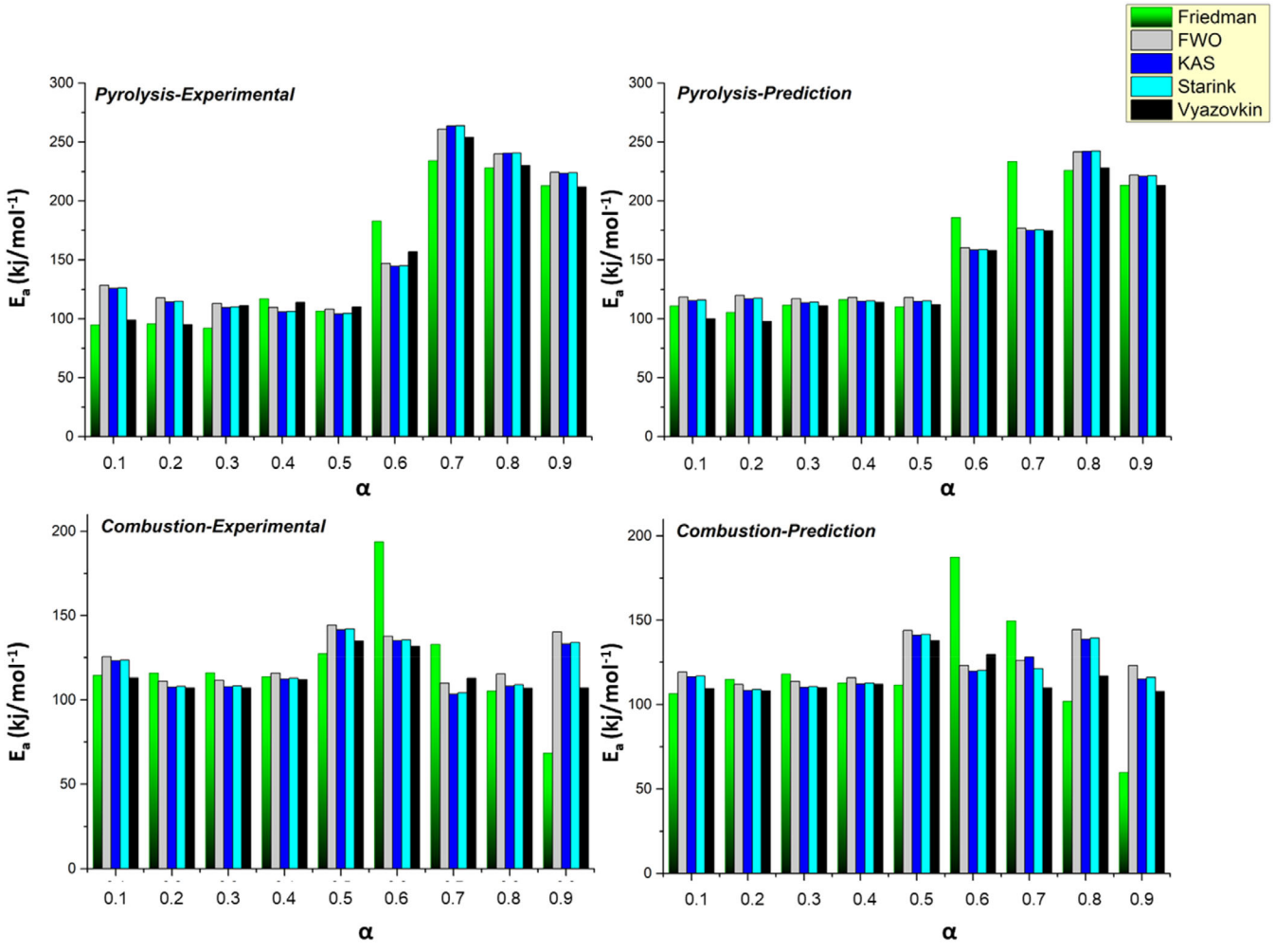

FIGURE 5 Comparison of activation energy results with the values calculated by advanced Vyazovkin method

Coats and Redfern model. On the other hand, Chen et al.[102] found activation energy of PVC between 45.7 and 185.0 using Coats and Redfern model. Another study by Han et al.[103] showed that activation energy during pyrolysis changed between 108.9 and 225.3 kJ/mol. A comparative study on PVC pyrolysis using FWO, KAS and Friedman methods resulted in activation energy ranges as 119.8–391.6, 110.7–378.6 and 76.9 and 608.5 kJ/mol, respectively, as it was reported by Pan et al.[104] When Yuan et al. used Distributed Activation Energy Model (DAEM) during the kinetic analysis of PVC, they calculated the activation energy between 102 and 272 kJ/mol.[105] Based on these previous kinetic studies, it is convenient to say that the properties and purity of the PVC sample, as well as the experimental and computational methodologies utilized, have a significant impact on kinetic analysis. Moreover, the atmosphere of thermal degradation has a marked effect on kinetics, as expected. A study of Han et al.[106] also agreed that the presence of oxygen during thermal decomposition of PVC affects mechanism and hence changes activation energy. For combustion, experimentally ant predictive average activation energy was found 120.8 and 118.0 kJ/mol, respectively, as it is observable in Table 4. In a study by Grammelis et. al[107] it is also found that activation energy of combustion is lower than that of activation energy of pyrolysis by using a parallel reaction model. Through the comparison of the activation energy, it is appropriate to conclude that the ANN model can give acceptable kinetic predictions, yielding a similar trend to the experimental data. Furthermore, both experimental and predicted data were analyzed using the more advanced Vyazovkin method in order to make a comparison to the other iso-conversional models, including Friedman, FWO, KAS and Starink. The estimated activation energy values were given in Table 5 and visualized in Figure 5. The activation energy calculated by the Vyazovkin method based on an advanced iso-conversional approach varied in the range of 95.2 to 253.9 kJ/mol with an average value of 153.5 kJ/mol using experimental data for pyrolysis, while ANN model resulted in average activation energy of 145.4 kJ/mol. On the other hand, lower values of average activation energy were obtained for combustion. The experimental and predicted values were 114.7 and 115.7 kJ/mol, respectively, for combustion of PVC using the Vyazovkin method. As seen in Figure 5, the values of activation energy with experimental data order and ANN model predictions followed a similar trend with deviations in the numerical values of activation energy at specified conversion degrees using kinetic models of Friedman, FWO, KAS, and Starink alongside Vyazovkin.

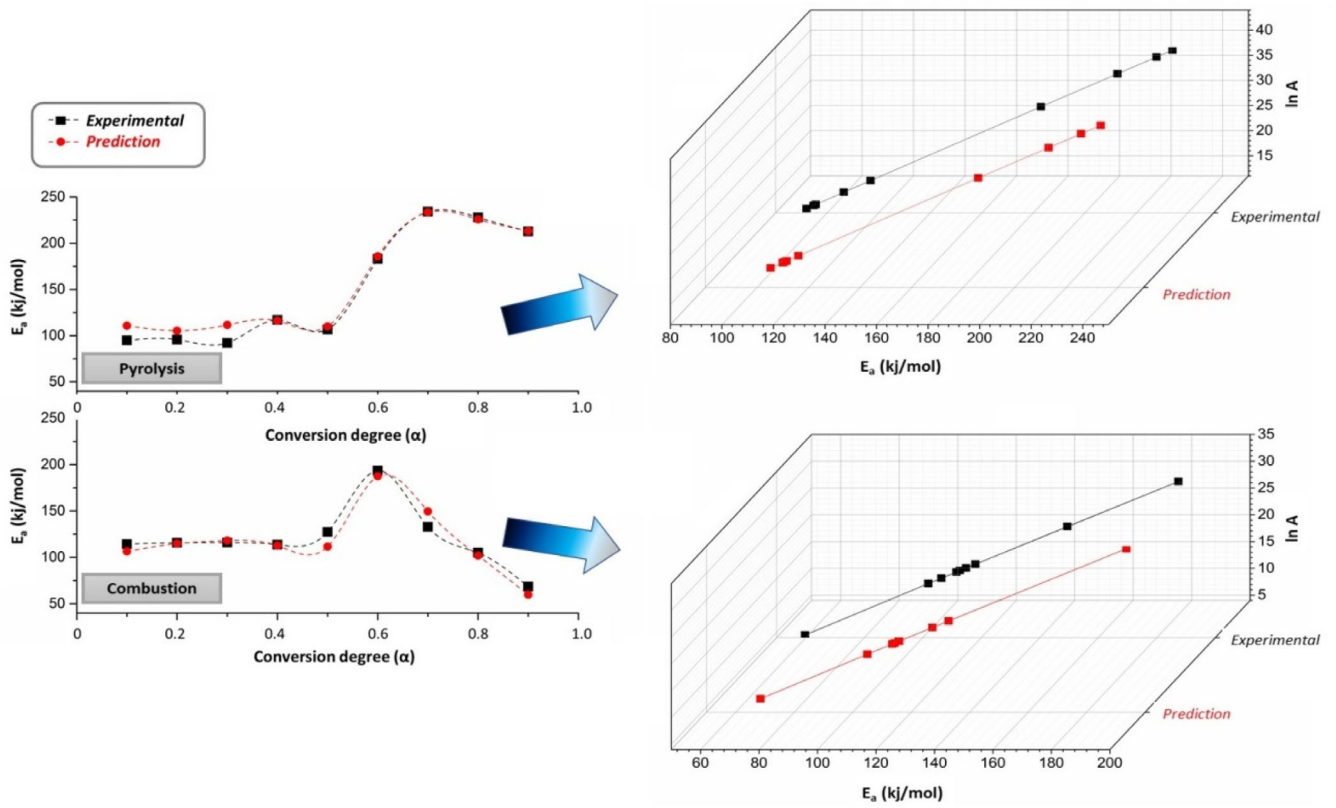

FIGURE 6 Assessment of activation energy with conversion degree and comparative compensation effect plots

The pre-exponential factor indicates intensity of collisions between activated molecules called an effective collision. Better reactivity in the same activation energy conditions is known to be a result of a more effective collision. The values of the pre-exponential factor during thermal pyrolysis and combustion elucidate the direct proportion to the complexity of PVC degradation. The values of the pre-exponential factor revealed the non-uniform thermal pattern throughout the pyrolytic and oxidative thermal degradation process of PVC. The pre-exponential factors of pyrolysis varied from 1.47×10^5 to 7.32×10^{18} s^{-1} by applying Friedman models with conversion degrees from 0.1 to 0.9. Otherwise, PVC combustion submitted pre-exponential factors between 9.12×10^1 and 2.55×10^{14} s^{-1}. The linear correlation between the lnA and E_a to facilitate the pyrolysis and combustion reaction of PVC is also shown in Figure 6. The plots of both pyrolysis and combustion yielded high regression coefficients which indicate strong linearity. To put it into other words, a perfect linear relationship between the activation energy and the pre-exponential factor values by an $\ln A = aEa + b$ type of mathematical expression can be applied for an energy compensation effect.[108,109] According to results, the relationship was found as $\ln A = 0.2220E_a$-8.5152 for pyrolysis and $\ln A = 0.2241E_a$-8.7511 for combustion. The estimated plot equations were also found similar to the experimentally obtained equations as given in Table 6. It can thus be apprehended that the ANN model used in this study possesses good kinetic prediction abilities and generalization performance in activation energy and pre-exponential factor relationship. As a consequence, ANN prediction for PVC pyrolysis and combustion agreed well with the kinetic results. Therefore, it is meaningful to rationalize these findings of the pyrolysis and combustion kinetics of PVC using ANN.

TABLE 6 Changes in pre-exponential factor as a function of conversion rate[a]

	Experimental		Prediction	
α	A (s^{-1})	Compensation plot equation	A (s^{-1})	Compensation plot equation
Pyrolysis				
0.1	2.72×10^5	$\ln A = 0.2220E_a$-8.5152	9.74×10^6	$\ln A = 0.2217E_a$-8.4491
0.2	3.29×10^5		2.91×10^6	
0.3	1.47×10^5		1.17×10^7	
0.4	3.93×10^7		3.26×10^7	
0.5	3.83×10^6		8.30×10^6	
0.6	9.46×10^{13}		1.76×10^{14}	
0.7	7.32×10^{18}		6.25×10^{18}	
0.8	1.85×10^{18}		1.18×10^{18}	
0.9	6.65×10^{16}		7.32×10^{16}	
$\bar{x}$	1.03×10^{18}		8.33×10^{17}	
Combustion				
0.1	3.73×10^6	$\ln A = 0.2241E_a$-8.7511	2.23×10^7	$\ln A = 0.2235E_a$-8.6682
0.2	2.49×10^7		3.05×10^7	
0.3	5.09×10^7		3.19×10^7	
0.4	1.55×10^7		1.90×10^7	
0.5	1.19×10^7		4.04×10^8	
0.6	2.55×10^{14}		9.99×10^{14}	
0.7	5.65×10^{10}		1.39×10^9	
0.8	1.36×10^6		2.76×10^6	
0.9	9.12×10^1		6.82×10^2	
$\bar{x}$	2.83×10^{13}		1.11×10^{14}	

Note: $\bar{x}$: Mean value.

[a]Calculations were based on Friedman method.

4 | CONCLUSIONS

The thermal degradation behavior of PVC has been predicted by developing an efficient ANN model under both inert and air atmospheres to assess its pyrolytic and combustive behavior. The following viewpoints can be used to explain the facts:

1. Introduction of oxygen into the degradation atmosphere resulted in different degradation tendencies. Fluctuations in the calculated instantaneous activation energy profiles concerning conversion degree suggested the multi-stage degradation of PVC under both nitrogen and air atmospheres.
2. R^2 scores of weight loss were calculated and found greater than 0.9977 for all datasets. In addition to R^2 scores, statistical analysis that utilized MSE, RMSE, and MAE has revealed the performance of the various ANN models in detail.
3. The results of ANN showed that the predicted kinetic parameters were reliable when the experimentally-found parameters have been considered. Put in other words, the ANN model showed good predictive capabilities when the parameters of the network are optimized and well-trained.

All in all, the findings of the current study confirm that the adopted experimental methodology based on thermogravimetry and ANN is suitable for proving valuable results for the kinetic modeling of complex non-linear systems. ANN provides a realistic approach to the design of thermochemical conversion processes. When PVC is utilized in industry, our modelling results aid in the selection of optimum conditions for obtaining precise pyrolysis and combustion kinetics. The use of PVC pyrolysis and combustion allows for the simulation of polymer-related thermal processes as well as the selection of optimal operating parameters. Future research should investigate the impact of pyrolysis and combustion process factors on activation energy to improve the feasibility of the thermochemical conversion methods by using ANN to predict the kinetics to reduce experimental efforts.

ACKNOWLEDGEMENTS

The authors appreciate the financial support from the Bilecik Şeyh Edebali University, Commission of Scientific Research Projects (Project no:2020-01.BŞEÜ.03-09 and 2019-02.BŞEÜ.03-03).

ORCID

Gamzenur Özsin https://orcid.org/0000-0001-5091-5485
Melis Alpaslan Takan https://orcid.org/0000-0002-1458-8162
Ayşe Eren Pütün https://orcid.org/0000-0002-2933-9804

REFERENCES

1. Heydariaraghi M, Ghorbanian S, Hallajisani A, Salehpour A. Fuel properties of the oils produced from the pyrolysis of commonly-used polymers: effect of fractionating column. *J Anal Appl Pyrolysis*. 2016;121:307-317.
2. Silva ALP. Increased plastic pollution due to COVID-19 pandemic: challenges and recommendations. *Chem Eng J*. 2020;405:126683.
3. Nižetić S, Djilali N, Papadopoulos A, Rodrigues JJPC. Smart technologies for promotion of energy efficiency, utilization of sustainable resources and waste management. *J Clean Prod*. 2019;231:565-591.
4. Gui B, Qiao Y, Wan D, et al. Nascent tar formation during polyvinylchloride (PVC) pyrolysis. *Proc Combust Inst*. 2013;34(2):2321-2329.
5. Dincer I, Rosen MA. A worldwide perspective on energy, environment and sustainable development. *Int J Energy Res*. 1998;22(15):1305-1321.
6. Özsin G, Pütün AE, Nakabayashi K, Miyawaki J, Yoon SH. Environmental-friendly production of carbon fiber from isotropic hybrid pitches synthesized from waste biomass and polystyrene with ethylene bottom oil. *J Clean Prod*. 2019;239:118025.
7. McIlveen-Wright D. A comparison of circulating fluidised bed combustion and gasification power plant technologies for processing mixtures of coal, biomass and plastic waste. *Fuel Process Technol*. 2006;87(9):793-801.
8. Hu Q, Tang Z, Yao D, Yang H, Shao J, Chen H. Thermal behavior, kinetics and gas evolution characteristics for the co-pyrolysis of real-world plastic and Tyre wastes. *J Clean Prod*. 2020;260:121102.
9. Sun K, Themelis NJ, Bourtsalas AC(T), Huang Q. Selective production of aromatics from waste plastic pyrolysis by using sewage sludge derived char catalyst. *J Clean Prod*. 2020;268:122038.
10. Vamvuka D. Bio-oil, solid and gaseous biofuels from biomass pyrolysis processes—an overview. *Int J Energy Res*. 2011;35(10):835-862.
11. Merdun H, Laougé ZB. Kinetic and thermodynamic analyses during co-pyrolysis of greenhouse wastes and coal by TGA. *Renew Energy*. 2021;163:453-464.
12. Abuadala A, Dincer I. A review on biomass-based hydrogen production and potential applications. *Int J Energy Res*. 2012;36(4):415-455.
13. Veksha A, Giannis A, Oh WD, Lisak G. Catalytic processing of non-condensable pyrolysis gas from plastics: effects of calcium supports on nickel-catalyzed decomposition of hydrocarbons and HCl sorption. *Chem Eng Sci*. 2018;189:311-319.
14. Song C, Zhang C, Zhang S, et al. Thermochemical liquefaction of agricultural and forestry wastes into biofuels and chemicals from circular economy perspectives. *Sci Total Environ*. 2020;749:141972.
15. Özsin G, Kılıç M, Apaydin-Varol E, Pütün AE, Pütün E. A thermo-kinetic study on co-pyrolysis of oil shale and polyethylene terephthalate using TGA/FT-IR. *Korean J Chem Eng*. 2020;37:1-11.
16. Sadat-Shojai M, Bakhshandeh G-R. Recycling of PVC wastes. *Polym Degrad Stab*. 2011;96(4):404-415.
17. Nadagouda MN, Pressman J, White C, Speth TF, McCurry DL. Novel thermally stable poly (vinyl chloride) composites for sulfate removal. *J Hazard Mater*. 2011;188(1–3):19-25.

18. Perera M, Ishiaku U, Ishak Z. Thermal degradation of PVC/-NBR and PVC/ENR50 binary blends and PVC/ENR50/NBR ternary blends studied by DMA and solid state NMR. *Polym Degrad Stab*. 2000;68(3):393-402.
19. Nair MR, Thomas GV, Nair MG. Thermogravimetric analysis of PVC/ELNR blends. *Polym Degrad Stab*. 2007;92(2):189-196.
20. Bhaskar T, Kaneko J, Muto A, et al. Pyrolysis studies of PP/-PE/PS/PVC/HIPS-Br plastics mixed with PET and dehalogenation (Br, cl) of the liquid products. *J Anal Appl Pyrolysis*. 2004;72(1):27-33.
21. Miranda R, Pakdel H, Roy C, Vasile C. Vacuum pyrolysis of commingled plastics containing PVC II. *Prod Anal Polym Degradat Stab*. 2001;73(1):47-67.
22. Ma S, Lu J, Gao J. Study of the low temperature pyrolysis of PVC. *Energy Fuel*. 2002;16(2):338-342.
23. O'Mara MM. High-temperature pyrolysis of poly (vinyl chloride): gas chromatographic-mass spectrometric analysis of the pyrolysis products from PVC resin and plastisols. *J polym Sci Part A-1: Polymer Chem*. 1970;8(7):1887-1899.
24. Zevenhoven R, Axelsen EP, Hupa M. Pyrolysis of waste-derived fuel mixtures containing PVC. *Fuel*. 2002;81(4):507-510.
25. Saeed L, Tohka A, Haapala M, Zevenhoven R. Pyrolysis and combustion of PVC, PVC-wood and PVC-coal mixtures in a two-stage fluidized bed process. *Fuel Process Technol*. 2004;85(14):1565-1583.
26. Hassan H, Hameed B, Lim J. Co-pyrolysis of sugarcane bagasse and waste high-density polyethylene: synergistic effect and product distributions. *Energy*. 2020;191:116545.
27. Qiao WM, Song Y, Yoon SH, Korai Y, Mochida I, Katou O. Preparation of PVC pitch from waste pipe. *Carbon*. 2005;43(9):2022-2025.
28. Liu J, Shimanoe H, Ko S, et al. Highly chlorinated polyvinyl chloride as a novel precursor for fibrous carbon material. *Polymers*. 2020;12(2):328.
29. Qiao WM, Yoon SH, Mochida I, Yang JH. Waste polyvinylchloride derived pitch as a precursor to develop carbon fibers and activated carbon fibers. *Waste Manag*. 2007;27(12):1884-1890.
30. Liu J. Preparation of isotropic pitch precursor for pitch-based carbon fiber through the co-carbonization of ethylene bottom oil and polyvinyl chloride. *J Ind Eng Chem*. 2018;67:276-283.
31. Qiao WM, Song Y, Yoon SH, et al. Carbonization of waste PVC to develop porous carbon material without further activation. *Waste Manag*. 2006;26(6):592-598.
32. Aguado R, Elordi G, Arrizabalaga A, Artetxe M, Bilbao J, Olazar M. Principal component analysis for kinetic scheme proposal in the thermal pyrolysis of waste HDPE plastics. *Chem Eng J*. 2014;254:357-364.
33. Varma AK, Lal N, Rathore AK, et al. Thermal, kinetic and thermodynamic study for co-pyrolysis of pine needles and styrofoam using thermogravimetric analysis. *Energy*. 2021;218:119404.
34. Narobe M, Golob J, Klinar D, Francetič V, Likozar B. Co-gasification of biomass and plastics: pyrolysis kinetics studies, experiments on 100 kW dual fluidized bed pilot plant and development of thermodynamic equilibrium model and balances. *Bioresour Technol*. 2014;162:21-29.
35. Lah B, Klinar D, Likozar B. Pyrolysis of natural, butadiene, styrene–butadiene rubber and Tyre components: modelling kinetics and transport phenomena at different heating rates and formulations. *Chem Eng Sci*. 2013;87:1-13.
36. Pomeroy B, Grilc M, Likozar B. Artificial neural networks for bio-based chemical production or biorefining: a review. *Renew Sustain Energy Rev*. 2022;153:111748.
37. Wang X, Yang J, Yang X, Hu X. A novel study on activated carbon production based on artificial neural network model: an experimental and artificial intelligence method approach. *Int J Energy Res*. 2022;1-17.
38. Zhao S, Xu W, Chen L. The modeling and products prediction for biomass oxidative pyrolysis based on PSO-ANN method: an artificial intelligence algorithm approach. *Fuel*. 2022;312:122966.
39. Sunphorka S, Chalermsinsuwan B, Piumsomboon P. Artificial neural network model for the prediction of kinetic parameters of biomass pyrolysis from its constituents. *Fuel*. 2017;193:142-158.
40. Naqvi SR, Hameed Z, Tariq R, et al. Synergistic effect on co-pyrolysis of rice husk and sewage sludge by thermal behavior, kinetics, thermodynamic parameters and artificial neural network. *Waste Manag*. 2019;85:131-140.
41. Gu C, Wang X, Song Q, Li H, Qiao Y. Prediction of gas-liquid-solid product distribution after solid waste pyrolysis process based on artificial neural network model. *Int J Energy Res*. 2021;45:13786-13800.
42. Yıldız Z, Uzun H, Ceylan S, Topcu Y. Application of artificial neural networks to co-combustion of hazelnut husk–lignite coal blends. *Bioresour Technol*. 2016;200:42-47.
43. Xie C, Liu J, Zhang X, et al. Co-combustion thermal conversion characteristics of textile dyeing sludge and pomelo peel using TGA and artificial neural networks. *Appl Energy*. 2018;212:786-795.
44. Govindan B, Chandra Babu Jakka S, Radhakrishnan TK, et al. Investigation on kinetic parameters of combustion and oxy-combustion of calcined pet coke employing thermogravimetric analysis coupled to artificial neural network modeling. *Energy Fuel*. 2018;32(3):3995-4007.
45. Shahbaz M, Taqvi SA, Minh Loy AC, et al. Artificial neural network approach for the steam gasification of palm oil waste using bottom ash and CaO. *Renew Energy*. 2019;132:243-254.
46. Conesa J, Caballero J, Reyes-Labarta J. Artificial neural network for modelling thermal decompositions. *J Anal Appl Pyrolysis*. 2004;71(1):343-352.
47. Bárbara DD, Araújo NR, Ligório RF, Pujatti FJ, Yoshida MI, Sebastião RC. Comparative kinetic study of automotive polyurethane degradation in non-isothermal and isothermal conditions using artificial neural network. *Thermochimica Acta*. 2018;666:116-123.
48. Dubdub I, Al-Yaari M. Pyrolysis of low density polyethylene: kinetic study using TGA data and ANN prediction. *Polymers*. 2020;12(4):891.
49. Yanik J, Uddin MA, Ikeuchi K, Sakata Y. The catalytic effect of red mud on the degradation of poly (vinyl chloride) containing polymer mixture into fuel oil. *Polym Degrad Stab*. 2001;73(2):335-346.

50. Zhou Q, Tang C, Wang YZ, Zheng L. Catalytic degradation and dechlorination of PVC-containing mixed plastics via Al–mg composite oxide catalysts. *Fuel*. 2004;83(13):1727-1732.
51. Tiikma L, Johannes I, Luik H. Fixation of chlorine evolved in pyrolysis of PVC waste by Estonian oil shales. *J Anal Appl Pyrolysis*. 2006;75(2):205-210.
52. Yu H, Qu J, Liu Y, et al. Co-pyrolysis of biomass and polyvinyl chloride under microwave irradiation: distribution of chlorine. *Sci Total Environ*. 2022;806:150903.
53. Haslam J, Soppet W. The determination of chlorine in resins obtained from polyvinyi chloride compositions. *J Soc Chem Ind*. 1948;67(1):33-35.
54. Altuğ M, Erdem M, Ozay C, Bozkır O. Surface roughness of Ti6Al4V after heat treatment evaluated by artificial neural networks. *Materials Testing*. 2016;58(3):189-199.
55. Altikat A, Alma MH. Application of new hybrid models based on artificial neural networks for modeling pyrolysis yields of Atriplex nitens S. *Int J Energy Res*. 2022;46(4):4445-4461.
56. Tufaner F, Demirci Y. Prediction of biogas production rate from anaerobic hybrid reactor by artificial neural network and nonlinear regressions models. *Clean Technol Env Policy*. 2020;22(3):713-724.
57. Yusri I, Majeed AA, Mamat R, Ghazali MF, Awad OI, Azmi WH. A review on the application of response surface method and artificial neural network in engine performance and exhaust emissions characteristics in alternative fuel. *Renew Sustain Energy Rev*. 2018;90:665-686.
58. Gulab H, Hussain K, Malik S, Hussain Z, Shah Z. Catalytic co-pyrolysis of Eichhornia Crassipes biomass and polyethylene using waste Fe and CaCO3 catalysts. *Int J Energy Res*. 2016;40(7):940-951.
59. Vamvuka D, Kakaras E, Kastanaki E, Grammelis P. Pyrolysis characteristics and kinetics of biomass residuals mixtures with lignite☆. *Fuel*. 2003;82(15–17):1949-1960.
60. Li M, Liu L, Jiang L, Gou FH, Sun JH. Application of distributed activation energy models to polymer pyrolysis: effects of distributed model selection, characteristics, validation, and sensitivity analysis. *Fuel*. 2019;254:115594.
61. Gerassimidou S, Velis CA, Williams PT, Komilis D. Characterisation and composition identification of waste-derived fuels obtained from municipal solid waste using thermogravimetry: a review. *Waste Manag Res*. 2020;38(9):942-965.
62. Liu L, Liu L, Zhang X, Zhao R, Song G, Tian L. Pyrolysis of Phragmites hirsuta study on pyrolysis characteristics, kinetic and thermodynamic analyses. *Int J Energy Res*. 2021;45(10):15200-15216.
63. de Caprariis B, Santarelli ML, Scarsella M, Herce C, Verdone N, de Filippis P. Kinetic analysis of biomass pyrolysis using a double distributed activation energy model. *J Thermal Analy Calorim*. 2015;121(3):1403-1410.
64. Roussi AT, Vouvoudi EC, Achilias DS. Pyrolytic degradation kinetics of HIPS, ABS, PC and their blends with PP and PVC. *Thermochimica Acta*. 2020;690:178705.
65. Mohamed M, Rashidi NA, Yusup S, Teong LK, Rashid U, Ali RM. Effects of experimental variables on conversion of cockle shell to calcium oxide using thermal gravimetric analysis. *J Clean Prod*. 2012;37:394-397.
66. Miranda M, Bica CI, Nachtigall SM, Rehman N, Rosa SM. Kinetical thermal degradation study of maize straw and soybean hull celluloses by simultaneous DSC–TGA and MDSC techniques. *Thermochimica Acta*. 2013;565:65-71.
67. Vyazovkin S, Burnham AK, Criado JM, Pérez-Maqueda LA, Popescu C, Sbirrazzuoli N. ICTAC kinetics committee recommendations for performing kinetic computations on thermal analysis data. *Thermochimica Acta*. 2011;520(1–2):1-19.
68. Vyazovkin S, Chrissafis K, di Lorenzo ML, et al. ICTAC kinetics committee recommendations for collecting experimental thermal analysis data for kinetic computations. *Thermochimica Acta*. 2014;590:1-23.
69. Vyazovkin S, Burnham AK, Favergeon L, et al. ICTAC kinetics committee recommendations for analysis of multi-step kinetics. *Thermochimica Acta*. 2020;689:178597.
70. Friedman HL. Kinetics of thermal degradation of char-forming plastics from thermogravimetry. Application to a Phenolic Plastic. *Journal of Polymer Science Part C: Polymer Symposia*. Hoboken: Wiley Online Library; 1964.
71. Ozawa T. A new method of analyzing thermogravimetric data. *Bull Chem Soc Jpn*. 1965;38(11):1881-1886.
72. Flynn JH, Wall LA. General treatment of the thermogravimetry of polymers. *J Res Natl Bur Stand*. 1966;70(6):487-523.
73. Kissinger HE. Reaction kinetics in differential thermal analysis. *Anal Chem*. 1957;29(11):1702-1706.
74. Akahira T, Sunose T. Method of determining activation deterioration constant of electrical insulating materials. *Res Rep Chiba Inst Technol (Sci Technol)*. 1971;16:22-31.
75. Starink M. A new method for the derivation of activation energies from experiments performed at constant heating rate. *Thermochimica Acta*. 1996;288(1–2):97-104.
76. Sahoo A, Saini K, Negi S, Kumar J, Pant KK, Bhaskar T. Inspecting the bioenergy potential of noxious Vachellia nilotica weed via pyrolysis: Thermo-kinetic study, neural network modeling and response surface optimization. *Renew Energy*. 2022;185:386-402.
77. Senum G, Yang R. Rational approximations of the integral of the Arrhenius function. *J Therm Analys Calorim*. 1977;11(3):445-447.
78. Cortés AM, Bridgwater A. Kinetic study of the pyrolysis of miscanthus and its acid hydrolysis residue by thermogravimetric analysis. *Fuel Process Technol*. 2015;138:184-193.
79. Drozin D, Sozykin S, Ivanova N, et al. Kinetic calculation: software tool for determining the kinetic parameters of the thermal decomposition process using the Vyazovkin method. *SoftwareX*. 2020;11:100359.
80. Pandey M, Joshi GM, Mukherjee A, Thomas P. Electrical properties and thermal degradation of poly (vinyl chloride)/-polyvinylidene fluoride/ZnO polymer nanocomposites. *Polymer Int*. 2016;65(9):1098-1106.
81. Ramesh S, Leen KH, Kumutha K, Arof AK. FTIR studies of PVC/PMMA blend based polymer electrolytes. *Spectrochim Acta A Mol Biomol Spectrosc*. 2007;66(4–5):1237-1242.
82. Lu P, Huang Q, Bourtsalas AC(T), Themelis NJ, Chi Y, Yan J. Review on fate of chlorine during thermal processing of solid wastes. *J Environ Sci*. 2019;78:13-28.
83. McNeill IC, Memetea L, Cole WJ. A study of the products of PVC thermal degradation. *Polym Degrad Stab*. 1995;49(1):181-191.
84. Wu C-H, Chang CY, Lin JP, Liang Y. Effects of hydrogen chloride on the pyrolysis of polyethylene: pyrolysis kinetics. *J Hazard Mater*. 1998;58(1–3):195-205.

85. Al-Sagheer F, Ahmad Z. Stabilizing poly (vinyl chloride) using its blends with poly (methyl methacarylate): pyrolysis GC/MS studies. *J Hazard Mater*. 2014;278:584-591.
86. Xie Q, Zhang H, Tong L. Experimental study on the fire protection properties of PVC sheath for old and new cables. *J Hazard Mater*. 2010;179(1–3):373-381.
87. Karayıldırım T, Yanık J, Yüksel M, Sağlam M, Haussmann M. Degradation of PVC containing mixtures in the presence of HCl fixators. *J Polym Environ*. 2005;13(4):365-374.
88. Li J, Dou B, Zhang H, Zhang H, Chen H, Xu Y. Thermochemical characteristics and non-isothermal kinetics of camphor biomass waste. *J Environ Chem Eng*. 2021;9(4):105311.
89. Valko L, Klein E, Kovařík P, Bleha T, Šimon P. Kinetic study of thermal dehydrochlorination of poly (vinyl chloride) in the presence of oxygen: III. Statistical thermodynamic interpretation of the oxygen catalytic activity. *Eur Polym J*. 2001;37(6):1123-1132.
90. Ye L, Li T, Hong L. Understanding enhanced char formation in the thermal decomposition of PVC resin: role of intermolecular chlorine loss. *Mater Today Commun*. 2021;26:102186.
91. Masuda Y, Uda T, Terakado O, Hirasawa M. Pyrolysis study of poly (vinyl chloride)–metal oxide mixtures: quantitative product analysis and the chlorine fixing ability of metal oxides. *J Anal Appl Pyrolysis*. 2006;77(2):159-168.
92. Aso H, Matsuoka K, Sharma A, Tomita A. Structural analysis of PVC and PFA carbons prepared at 500–1000 C based on elemental composition, XRD, and HRTEM. *Carbon*. 2004;42(14):2963-2973.
93. Xia Z, Yang H, Sun J, Zhou Z, Wang J, Zhang Y. Co-pyrolysis of waste polyvinyl chloride and oil-based drilling cuttings: pyrolysis process and product characteristics analysis. *J Clean Prod*. 2021;318:128521.
94. Wienchol P, Szlęk A, Ditaranto M. Waste-to-energy technology integrated with carbon capture–challenges and opportunities. *Energy*. 2020;198:117352.
95. Bittencourt PRS, Scremin FR. Evolved gas analysis of PE: PVC systems thermodegradation under inert and oxidizing atmosphere. *J Polym Environ*. 2019;27(3):612-617.
96. Liu H, Liu J, Huang H, Evrendilek F, He Y, Buyukada M. Combustion parameters, evolved gases, reaction mechanisms, and ash mineral behaviors of durian shells: a comprehensive characterization and joint-optimization. *Bioresour Technol*. 2020;314:123689.
97. Özsin G, Apaydın-Varol E, Kılıç M, Pütün AE, Pütün E. Pyrolysis of petroleum sludge under non-isothermal conditions: thermal decomposition behavior, kinetics, thermodynamics, and evolved gas analysis. *Fuel*. 2021;300:120980.
98. SP SP, Swaminathan G, Joshi VV. Thermogravimetric analysis of hazardous waste: pet-coke, by kinetic models and artificial neural network modeling. *Fuel*. 2021;287:119470.
99. Coulibaly P, Baldwin CK. Nonstationary hydrological time series forecasting using nonlinear dynamic methods. *J Hydrol*. 2005;307(1–4):164-174.
100. Liu H, Wang C, Zhang J, Zhao W, Fan M. Pyrolysis kinetics and thermodynamics of typical plastic waste. *Energy Fuel*. 2020;34(2):2385-2390.
101. Xu F, Wang B, Yang D, Hao J, Qiao Y, Tian Y. Thermal degradation of typical plastics under high heating rate conditions by TG-FTIR: pyrolysis behaviors and kinetic analysis. *Energ Conver Manag*. 2018;171:1106-1115.
102. Chen R, Zhang S, Yang X, et al. Thermal behaviour and kinetic study of co-pyrolysis of microalgae with different plastics. *Waste Manag*. 2021;126:331-339.
103. Han B, Chen Y, Wu Y, et al. Co-pyrolysis behaviors and kinetics of plastics–biomass blends through thermogravimetric analysis. *J Thermal Anal Calorim*. 2014;115(1):227-235.
104. Pan J, Jiang H, Qing T, Zhang J, Tian K. Transformation and kinetics of chlorine-containing products during pyrolysis of plastic wastes. *Chemosphere*. 2021;284:131348.
105. Yuan Z, Zhang J, Zhao P, et al. Synergistic effect and chlorine-release behaviors during co-pyrolysis of LLDPE, PP, and PVC. *ACS Omega*. 2020;5(20):11291-11298.
106. Han, B., Wu Y.L., Feng W., Chen Z., Yang M.D. Kinetic study of PVC pyrolysis in air by Thermogravimetric analysis using the Friedman method. *Adv Mater Res*. 2012. Trans Tech Publ, 427, 64, 69.
107. Grammelis P, Basinas P, Malliopoulou A, Sakellaropoulos G. Pyrolysis kinetics and combustion characteristics of waste recovered fuels. *Fuel*. 2009;88(1):195-205.
108. Skodras G, Grammelis P, Basinas P, Kakaras E, Sakellaropoulos G. Pyrolysis and combustion characteristics of biomass and waste-derived feedstock. *Ind Eng Chem Res*. 2006;45(11):3791-3799.
109. Özsin G, Dermenci KB, Turan S. Thermokinetic and thermodynamics of Pechini derived Li 7–3 × Al × La 3 Zr 2 O 12 (X = 0.0–0.2) xerogel decomposition under oxidative conditions. *J Thermal Anal Calorim*. 2021;146:1405-1420.

SUPPORTING INFORMATION

Additional supporting information can be found online in the Supporting Information section at the end of this article.

How to cite this article: Özsin G, Alpaslan Takan M, Takan A, Pütün AE. A combined phenomenological artificial neural network approach for determination of pyrolysis and combustion kinetics of polyvinyl chloride. *Int J Energy Res*. 2022;46(12):16959-16978. doi:10.1002/er.8361